

Dielectron production in pion-nucleon reactions and form factor of baryon transition within the time-like region

A.P.Jerusalimov, G.I.Lykasov

Joint Institute for Nuclear Research, 141980 Dubna, Russia

Abstract

Dielectron production in reactions $\pi^-p \rightarrow ne^+e^-$ and $\pi^-p \rightarrow ne^+e^-\gamma$ at energies less than 1 GeV is studied assuming electron-positron pair production to occur in the virtual time-like photon splitting process. Theoretical predictions of the effective mass distribution of dielectrons and their angular dependence are presented. Extraction of the electromagnetic form factor of baryon transition in the time-like region from future experiments of the HADES Collaboration is discussed.

1. Introduction

Investigation of the electromagnetic form factor (FF) of hadrons provides significant information about their structure. For example, measurement of the $e^+e^- \rightarrow \pi^+\pi^-$ cross section results in the pion FF in the time like region, which results in parameters of the ρ -meson and its excited states. This cross section has been measured in Orsay [1], Novosibirsk [2]-[4], Frascati (KLEO) [5], SLAC (BABAR) [6, 7] and Beijing (BESIII) [8].

There is another way to investigate the electromagnetic form factor in time-like four-momentum space in processes of e^+e^- -pair production in hadron-hadron, hadron-nucleus and nucleus-nucleus collisions with the High Acceptance Di-Electron Spectrometer (HADES) [9]. Experimental [10, 11] and theoretical [12]-[19] analysis of dielectron production in pp, np, pA and AA collisions leads to detailed information on the reaction mechanism, which is due mainly to the creation of baryonic and mesonic resonances in the intermediate state decayed into e^+e^- -pair. The study of exclusive dielectron production in meson-nucleon interaction at not large initial energies, for example, at about a few hundred MeV simplifies the theoretical analysis because the number of baryonic and mesonic resonances in the intermediate state is not large. In this case the e^+e^- production in πN interaction can be studied assuming the electron-positron pair to be produced in the virtual time-like photon splitting and to be considered a e^+e^- dipole. From future experimental data on $\pi^-p \rightarrow \gamma^*n \rightarrow e^+e^-n$ planned at HADES [24] interesting information about this e^+e^- dipole, for example, its form factor can be found. In this paper we continue our previous theoretical analysis of the reaction $\pi^-p \rightarrow e^+e^-n$ [20] at intermediate energies less than 1 GeV. In addition to that we include the contributions of a few additional channels, namely, $\pi^-p \rightarrow \pi^0n \rightarrow e^+e^-\gamma n$, $\pi^-p \rightarrow \rho^0n \rightarrow e^+e^-n$ and

$\pi^- p \rightarrow \eta^0 n \rightarrow e^+ e^- \gamma n$, which increase the dielectron effective mass distribution and result in predictions of the future HADES experiment for the form factor of the $e^+ e^-$ dipole. ‘

2. General formalism

We analyze the reaction $\pi N \rightarrow \gamma^* N \rightarrow e^+ e^- N$ within the unified model. This means that in the one-photon approximation, owing to T -invariance, three reactions $\gamma N \rightarrow \pi N, e N \rightarrow e \pi N$ and $\pi N \rightarrow e^+ e^- N$ are related to the process $\gamma^* N \leftrightarrow \pi N$ by the hadron current $J_\mu(s, t, m_\gamma^2)$, where $m_\gamma^2 = 0, > 0$ and $m_\gamma^2 < 0$ correspond to pion photoproduction, electroproduction and inverse pion electroproduction (IPE), respectively [21, 22]. In our previous paper [20] application of this unified model to calculate the $e^+ e^-$ effective mass distribution and the angular distribution of the virtual photon decayed into $e^+ e^-$ in the IPE processes was presented in detail. A satisfactory description of the data at a pion initial momentum of about 300 MeV/c was presented. Therefore, we shall omit the details of the matrix element calculation for reaction $\pi^- p \rightarrow \gamma^* n \rightarrow e^+ e^- n$ and only present the general forms for the effective mass distribution $d\sigma/dM_{e^+e^-}$ of the $e^+ e^-$ pair and the angular distribution $d\sigma/d \cos \theta_{\gamma^*}^*$ of the virtual γ^* in the $\pi - N$ c.m.s.[20]:

$$\frac{d\sigma}{dM_{e^+e^-}} = \frac{\alpha_{em}^2}{12\pi M_{e^+e^-} s \lambda^{1/2}(s, \mu_\pi^2, m^2)} \int_{t^-}^{t^+} \frac{\lambda^{1/2}(s, q^2, m^2)}{s} (FF(q^2))^2 \sum_{spins} J_\mu J_\nu^+ dt ; \quad (1)$$

$$\frac{d\sigma}{d \cos \theta_{\gamma^*}^*} = \frac{\alpha_{em}^2}{48\pi s \lambda^{1/2}(s, \mu_\pi^2, m^2)} \int \frac{\lambda^{1/2}(s, q^2, m^2)}{q^2} (FF(q^2))^2 \sum_{spins} J_\mu J_\nu^+ dq^2 , \quad (2)$$

where $\alpha_{em} = e^2/4\pi = 1/137$; $\lambda(x^2, y^2, z^2) = (x^2 - (y + z)^2)(x^2 - (y - z)^2)$ and $\sum_{spins} J_\mu J_\nu^+ = W_{\mu\nu}$ is the hadronic tensor, which was calculated in [20] including the graphs of Figs. (1,2). Let us note that the contribution of the t -channel one exchange graph Fig. (2a) to $d\sigma/dM_{ee}$ is very small at initial momenta less than 1GeV/c, see, for example, [23] and references therein, compared to contributions of the one baryonic exchange in the s -channel (Fig. (1a)) and in u -channel (Fig.(1b)). At initial pion momenta of about 300 MeV/c the graphs of Fig. (1) with the Δ -isobar exchange result in the main contribution to $d\sigma/dM_{e^+e^-}$. At higher initial momenta up to 700-800 MeV/c, which correspond to the HADES experiment with the pion beam [24], the additional graphs corresponding to the production of ρ^0 and η^0 , can contribute to the matrix element of this reaction. They are presented in Fig. (3). The contributions of these graphs with the exchange of different baryonic resonances were calculated within the Generalized Isobar Model (GIM) [25, 26], see APPENDIX.

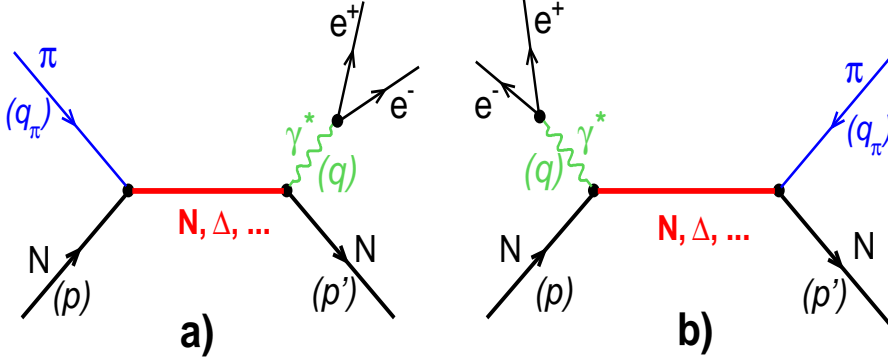


Figure 1: The one-nucleon or one-nucleon resonance exchange graph in the s -channel (a) and u -channel (b) of the IPE $\pi N \rightarrow \gamma N \rightarrow e^+e^-N$ process.

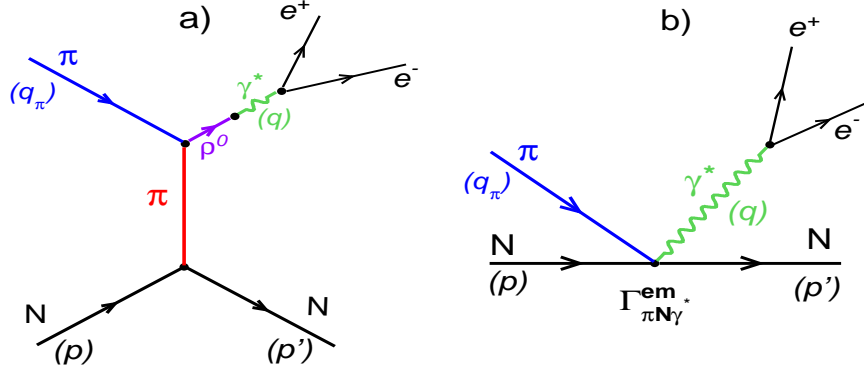


Figure 2: The one-pion exchange graph in the t -channel (a) and the electromagnetic contact term (b) for the IPE.

3. Electromagnetic form factor at the time-like region

As it was mentioned above, the pion form factor F_π in the time-like region was measured directly in the annihilation process $e^+e^- \rightarrow \pi^+\pi^-$ from its cross section. Then, the mean value of the pion radius square was determined from F_π as follows [2, 8]:

$$\langle r_\pi^2 \rangle = 6 \frac{dF_\pi(s)}{ds} \Big|_{s=0}, \quad (3)$$

where s is the square of the initial energy in the c.m.s of e^+e^- . According to [2], $\langle r_\pi^2 \rangle = 0.422 \pm 0.003 \pm 0.0013 \text{ fm}^2$. The mean square radius of the charged ρ -meson, which can be determined, for example, from its decay constant [27], is, about $0.56\text{-}0.6 \text{ fm}^2$, i.e., larger than the similar value for a pion.

To include the virtual photon off-shellness in our process $\pi^-p \rightarrow \gamma^*n \rightarrow e^+e^-n$, which can be large, up to about a few hundred MeV, we introduced the electromag-

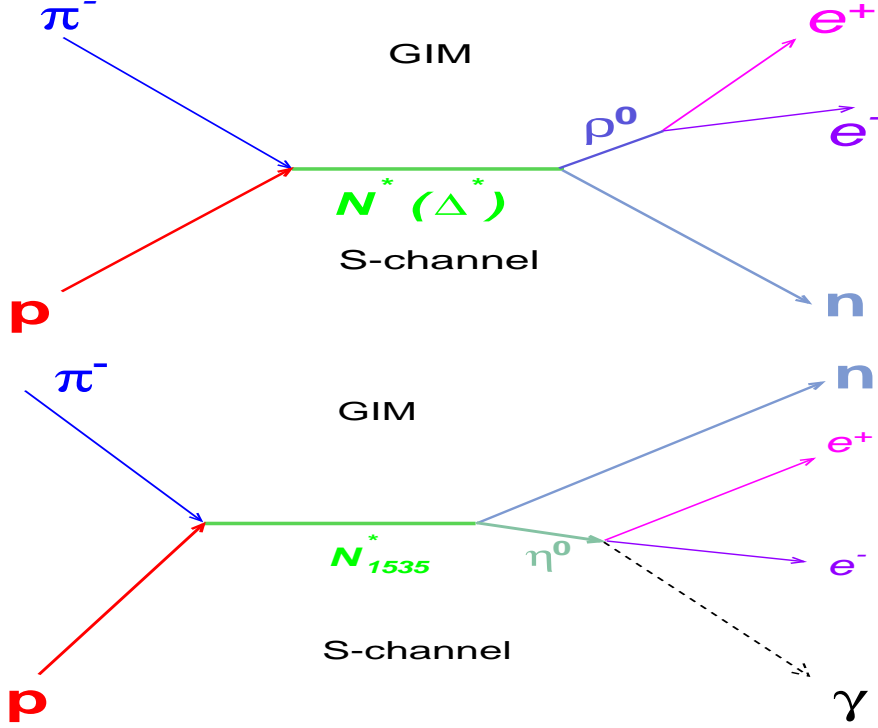


Figure 3: The one-nucleon resonance exchange graph in the s -channel of the IPE with production of $\rho^0 \rightarrow e^+e^-$ (top) and $\eta^0 \rightarrow e^+e^-\gamma$ (bottom).

netic form factor $FF(q^2)$ in Eqs. (1,2). We choose this FF in two forms:

$$FF(q^2) = \frac{\Lambda^2}{\Lambda^2 - q^2} \quad (4)$$

and

$$FF(q^2) = \exp(R^2 q^2) \quad (5)$$

For the virtual photon in the time-like region, when $q^2 > 0$, the form factor FF can become larger than 1, therefore, it increases the M_{ee} -spectrum at large $q^2 = M_{ee}^2$. Actually, the FF in the form of Eq.(4) is similar to the form factor corresponding to the vector meson dominance model (VMD), when the parameter Λ is the vector meson mass M_V . In order to avoid the divergence in Eq.(4) at $q^2 = \Lambda^2$ we also use the exponential form of FF (Eq. (5)). The e^+e^- pair in the s -channel (Fig. (1)) is produced from the baryonic transition in the time-like region, and the form factor $FF(q^2)$ can determine the size of this region. This form factor FF can be extracted from future HADES experimental data on $d\sigma/dM_{e^+e^-}$ and $d\sigma/d\cos\theta_{\gamma^*}^*$ in a similar way, as it was done for the pion FF from the $e^+e^- \rightarrow \pi^+\pi^-$ cross section [2, 8]. The mean value of the square radius of the electromagnetic baryonic transition (BT) is

related to the derivative of FF like in Eq. (3)

$$\langle r_{BT}^2 \rangle = 6 \frac{dFF}{dq^2} \Big|_{q^2=0} \quad (6)$$

So, knowing the FF from future experiments on $\pi^-p \rightarrow e^+e^-n$ one can estimate the size of the time-like baryonic transition region.

4. Results and discussion

We have calculated the distributions of e^+e^- pairs as functions of the dielectron effective mass $M_{e^+e^-}$ and $\cos\theta_{\gamma^*}$ for the processes $\pi^-p \rightarrow \gamma^*n \rightarrow e^+e^-n$ and $\pi^-p \rightarrow \gamma^*n \rightarrow e^+e^-n\gamma$ at initial pion momenta from a few hundred MeV/c up to 1 GeV/c. In Fig. (4) we present the distribution $d\sigma/dM_{ee}$ for these processes denoted as $\pi^-p \rightarrow \gamma^*n \rightarrow e^+e^-n(\gamma)$ at the initial pion momentum $P_{in} = 683$ MeV/c corresponding to the HADES experiment. The blue long dashed line in Fig. (4) corresponds to reaction $\pi^-p \rightarrow \gamma^*n \rightarrow e^+e^-n$ inputting the form factor $FF = 1$; the green long dashed-dotted curve corresponds to the channel $\pi^-p \rightarrow \pi^0n \rightarrow e^+e^-n\gamma$; the red short dashed-dotted line and the red dotted curves correspond to the contributions of channels $\pi^-p \rightarrow n\eta^0 \rightarrow e^+e^-n\gamma$ and $\pi^-p \rightarrow \rho^0n \rightarrow e^+e^-n$, respectively. At the HADES facility it is very difficult to distinguish the channel $\pi^-p \rightarrow e^+e^-n$ from the channel $\pi^-p \rightarrow e^+e^-n\gamma$, therefore, we incoherently sum up the contributions of these four channels presented by open black circles in Fig. (4) inputting $FF = 1$. The M_{ee} -spectrum for this sum is denoted as the spectrum of the process $\pi^-p \rightarrow e^+e^-n(\gamma)$. Then, we investigate the sensitivity of our results to the form factor FF chosen in the Gaussian form given by Eq. (5). The solid line in Fig. (4) is the total M_{ee} -spectrum including all these channels and inputting in the form factor FF the parameter $R = 1.6$ (GeV/c) $^{-1} = 0.32$ fm., which corresponds to the square ρ -meson radius of about 0.614 fm 2 [27]. The crosses in Fig. (4) are our calculations of the spectrum for the parameter $R = 3$ (GeV/c) $^{-1}$, which corresponds to the square radius $\langle r_{BT}^2 \rangle$ of about 2 fm 2 . Let us note that the proton charge radius $R_E \simeq 0.841$ fm. and the proton magnetic radius $R_M = 0.87$ fm. and the Zemach radius $R_Z = 1.082$ fm., which reflects the spatial distribution of magnetic moments smeared out by the charge distribution of the proton [28]. The sensitivity of the total M_{ee} -spectrum to the parameter R was presented in detail in Fig. (5). One can see an enhancement in the spectrum at $M_{ee} > 300$ MeV/c 2 at large values of the parameter R . This enhancement could be due to a big off-shellness of the virtual photon γ . An excess of this spectrum over our calculations performed without the form factor FF can provide information on the form factor FF of electromagnetic baryon transition. Therefore, the future exclusive HADES experiments on the dielectron production in pion-proton and pion-nucleus interactions one can permit to estimate the the size of the time-like baryon transition to e^+e^-N , according to Eq. (6).

In Fig. (6) we present the cross section of the process $\pi^-p \rightarrow e^+e^-n(\gamma)$ as a

function of the initial pion momentum. The notations are the same as in Fig. (4) and the calculations were performed at $R = 1.6 \text{ (GeV/c)}^{-1} = 0.32 \text{ fm}$.

In Fig. (7) the angular distribution $d\sigma/d\cos\theta_{\gamma^*}$ is presented at $P_{in} = 683 \text{ MeV/c}$ and $R = 1.6 \text{ (GeV}^{-1} =) 0.32 \text{ fm}$. integrated over $q^2 = M_{ee}^2$. As our calculations show, this distribution is practically not sensitive to the inclusion of FF . One can see the asymmetry of distribution $d\sigma/d\cos\theta_{\gamma^*}$, which depends on the initial momentum very weakly, according to our calculations.

In Fig. (8, left) the angular distribution $d\sigma/d\cos\theta_{\gamma^*}$ is presented for reaction $\pi^-p \rightarrow e^+e^-n$ at $P_{in} = 300 \text{ MeV/c}$ and $0.046(\text{GeV/c})^2 \leq q^2 \leq 0.065(\text{GeV/c})^2$ obtained in [20]. The experimental data are taken from [29]. The solid curve corresponds to our calculations, e.g., the coherent sum of the one-nucleon and Δ -exchange graphs with the positive phase sign of the second graph. In Fig. (8, right) the similar angular distribution is presented for $P_{in} = 683 \text{ MeV/c}$ and the same interval of q^2 . We present Fig. (8) to illustrate the similarity of such distributions at different initial momenta.

5. Conclusion

In this paper we have continued to analyze inverse pion electroproduction (IPE) processes $\pi p \rightarrow e^+e^-n$ at intermediate energies considered in [20]. In addition to that we have calculated the contributions of channels $\pi^-p \rightarrow \pi^0n \rightarrow e^+e^-\gamma n$, $\pi^-p \rightarrow \eta^0n \rightarrow e^+e^-\gamma n$ and $\pi^-p \rightarrow \rho^0n \rightarrow e^+e^-n$ to the effective mass distribution of dielectrons produced in the π^-p process including the final photon γ , which is not detected at the HADES facility. Therefore, we analyzed the process $\pi^-p \rightarrow \pi^0n \rightarrow e^+e^-n(\gamma)$ and investigated the sensitivity of observables, namely, the e^+e^- effective mass distribution $d\sigma/dM_{e^+e^-}$ and the angular distribution $d\sigma/d\cos\theta_{\gamma^*}$ to the electro-magnetic form factor FF given by Eq. (5). We found that the inclusion of this form factor by calculation of the effective mass distribution of the e^+e^- pair can result in an enhancement in this spectrum at $M_{ee} > 300 \text{ MeV/c}^2$, which could be due to the electromagnetic properties of the time-like baryon transition. It can be verified by incoming HADES experiment.

Acknowledgements. We are grateful to T.Galatyuk, R.Holzman, V.P. Ledygin, D.Nitt, G.Pontecorvo, V.Pechenov, B.Ramstein, A.Rustamov, P.Salabura, J.Stroth for very useful discussions.

6. Appendix: Parametrization of $\pi N \rightarrow \rho N$ (ηN) reactions

Within the Generalized Isobar Model (GIM) [25, 26] $\pi N \rightarrow \pi\pi N$ reactions are described as quasi-two body reactions ($a + b \rightarrow c + d$):

$$\pi N \rightarrow N^*(\Delta^*) \rightarrow N\rho^0$$

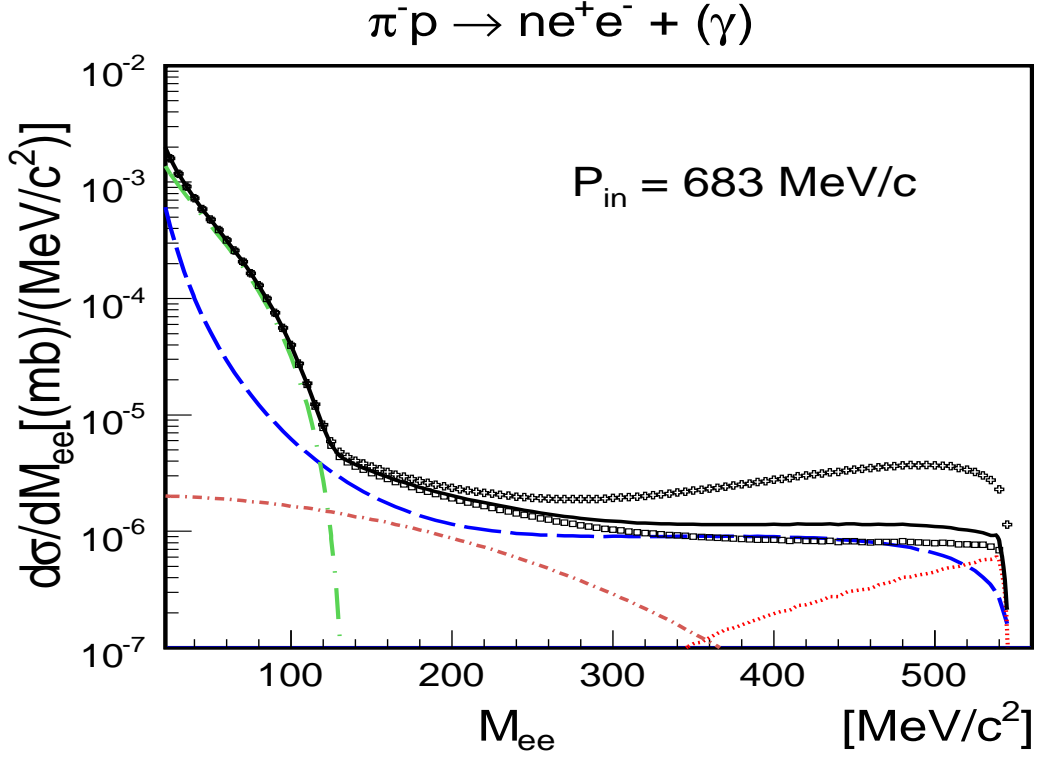


Figure 4: Invariant mass distribution for dielectrons, $d\sigma/dM_{e^+e^-}$, produced in the reaction $\pi^- p \rightarrow e^+ e^- n(\gamma)$. The solid curve corresponds to our total calculation including the exponential form factor in the form of Eq. 5 at $R = 1.6 \text{ (GeV}/c)^{-1}$; the open circles correspond to the same calculation but at $R = 0$ and the crosses are our total calculation at $R = 3 \text{ GeV}/c)^{-1}$. The separate contributions to this spectrum are presented by the blue long dashed line (the channel $\pi^- p \rightarrow e^+ e^- n$), the green long dashed-dotted line ($\pi^- p \rightarrow n\pi^0 \rightarrow ne^+e^-\gamma$), the red short dashed-dotted curve (the channel $\pi^- p \rightarrow n\eta^0 \rightarrow ne^+e^-\gamma$, Fig. (3 bottom)) and the red dotted line (the channel $\pi^- p \rightarrow n\rho^0 \rightarrow ne^+e^-$, Fig. (3 top)).

$$\pi N \rightarrow N^*(\Delta^*) \rightarrow N\eta^0$$

with the subsequent decays:

$$\rho \rightarrow e^+e^-,$$

$$\eta^0 \rightarrow e^+e^-\gamma.$$

The parameters of the following resonances (**** and ***) were taken from the

$\pi^- p \rightarrow n e^+ e^- + (\gamma)$ at $P_{in} = 683 \text{ MeV}/c$

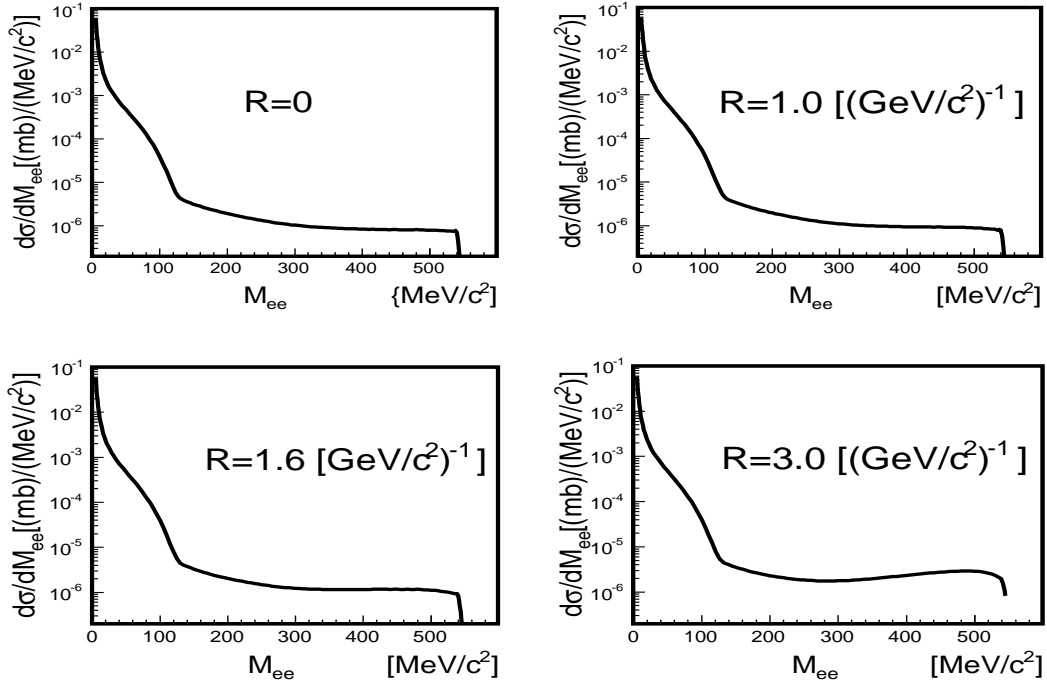


Figure 5: Invariant mass distribution for dielectrons, $d\sigma/dM_{e^+e^-}$, produced in the reaction $\pi^- p \rightarrow e^+ e^- n$ calculated by including the form factor FF in the form of Eq. 5 at different values of parameter R .

Review of Particle Properties:

| | |
|----------------|----------------|
| $N^*(1440)P11$ | $D^*(1600)P33$ |
| $N^*(1520)D13$ | $D^*(1620)S31$ |
| $N^*(1675)D15$ | $D^*(1700)D33$ |
| $N^*(1680)F15$ | $D^*(1900)S31$ |
| $N^*(1720)P13$ | $D^*(1905)F35$ |
| $N^*(2000)F15$ | $D^*(1910)P31$ |
| $N^*(2080)D13$ | $D^*(1920)P33$ |
| $N^*(2190)G17$ | $D^*(1940)D33$ |
| | $D^*(1950)F37$ |

The spin and isospin relations were taken account.

For quasi two-body reactions like $a + b \rightarrow c + d$ one can write

$$d\sigma = \frac{1}{(2S_a + 1)(2S_b + 1)} \left(\frac{2\pi}{p} \right)^2 \sum_{\lambda_i} | \langle \lambda_d \lambda_c | T | \lambda_b \lambda_a \rangle |^2 \times dPS,$$

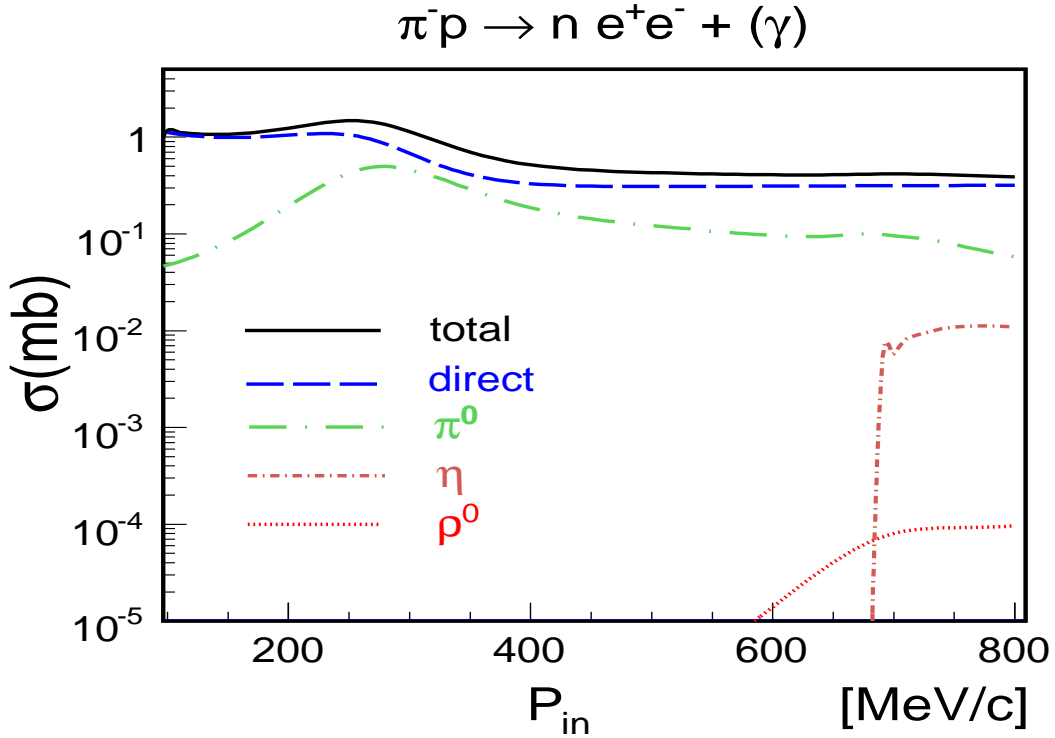


Figure 6: The cross section of the process $\pi^- p \rightarrow e^+ e^- n(\gamma)$ as a function of the initial pion momentum. The notations are the same as in Fig. 4 and the calculations were performed at $R = 1.6 \text{ (GeV/c)}^{-1} = 0.32 \text{ fm}$.

$$\langle \lambda_d \lambda_c | T | \lambda_b \lambda_a \rangle = \frac{1}{4\pi} \sum_j (2j+1) \langle \lambda_d \lambda_c | T_j | \lambda_b \lambda_a \rangle e^{i(\lambda-\mu)\varphi} d_{\lambda\mu}^j(\theta).$$

where $\lambda = \lambda_a - \lambda_b$, $\mu = \lambda_c - \lambda_d$ are helicity variables,
 $d_{\lambda\mu}^j(\theta)$ is the rotation matrix,
 dPS is the phase space element.

The angular distribution for the outgoing mesons (ρ and η) in CMS is the following:

$$\frac{d\sigma}{d\Omega} \sim \text{const} \times BW(\sqrt{s}, M_R, \Gamma_R)$$

References

- [1] J.E. Augustin, et al., Phys.Rev.Lett. **20**, 126 (1968).
- [2] L.M. Barkov, et al., Nucl.Phys. **B256**, 365 (1985).
- [3] R.R. Akhmetshin, et al., CMD2 Collaboration, Phys.Lett. B **578**, 285 (2004).

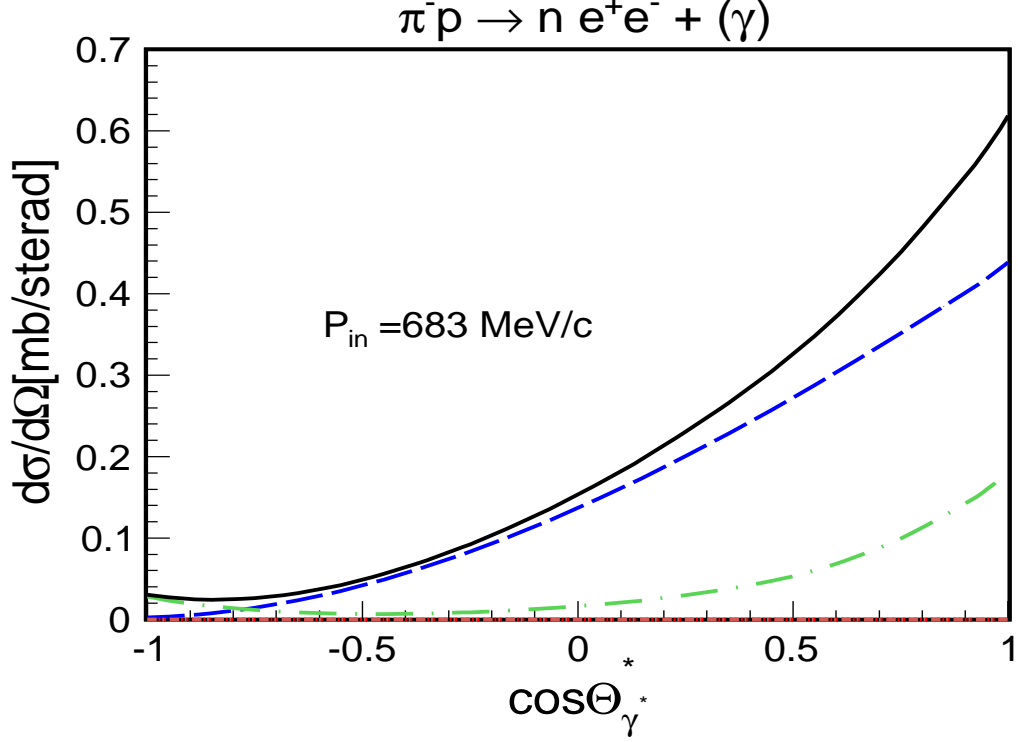


Figure 7: Angular distribution $d\sigma/d\cos\theta_{\gamma^*}$, where θ_{γ^*} is the angle of the virtual photon γ^* . The calculations were performed at $P_{in} = 683 \text{ MeV}/c$ and $R = 1.6$ ($\text{GeV}^{-1} = 0.32 \text{ fm}$).

- [4] . R.R. Akhmetshin, et al., CMD2 Collaboration, Phys.Lett. B **648**, 28 (2007).
- [5] D. Babusci, et al., KLOE collaboration, Phys.Lett. B **720**, 336 (2013).
- [6] B. Aubert, et al., BABAR Collaboration, Phys.Rev.Lett. **103**, 231801 (2009).
- [7] J.P. Less, et al., BABAR Collaboration, Phys.Rev. D **86**, 032013 (2012).
- [8] M. Ablikim et al., BESIII Collaboration, Phys.Lett. B **753**, 629 (2016).
- [9] G. Agakishiev et al., HADES Collaboration, Eur.Phys.J. A**41**, 243 (2009).
- [10] G. Agakishiev et al., HADES Collaboration, Phys.Lett. B **690**, 118 (2010).
- [11] G. Agakishiev et al., HADES Collaboration, Eur.Phys.J. A**53**, 149 (2017).
- [12] D.A. Gaffen, Phys.Rev. C **125**, 1745 (1962).
- [13] Rekalov M.P., Sov.J.Nucl.Phys. **1**, 760 (1965).
- [14] E.L. Bratkovskaya, W. Cassing and U. Mosel, Nucl.Phys. A **686**, 568 (2001).

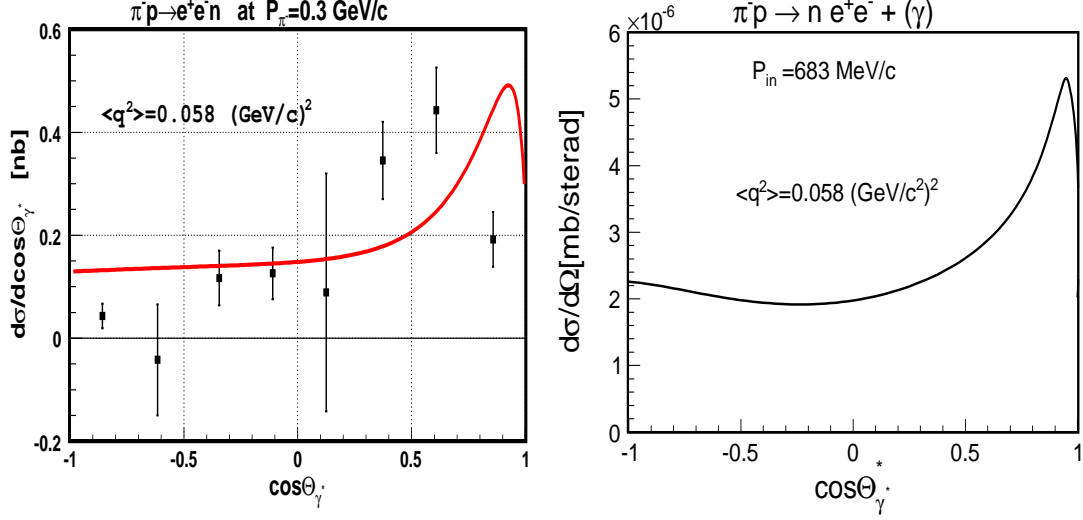


Figure 8: Left: angular distribution $d\sigma/d\cos\theta_{\gamma^*}$ for $\pi^-p \rightarrow e^+e^-n$ at initial pion momentum $P_\pi = 300$ MeV/c [20] and $\langle q^2 \rangle = 0.058$ (GeV/c) 2 . where θ_{γ^*} is the angle of the virtual photon γ^* . The solid curve corresponds to our calculations [20], the experimental data are taken from [29]. Right: the same angle distribution, as the one presented to the left but at $P_\pi = 683$ MeV/c.

- [15] E.L. Bratkovskaya, W. Cassing, Nucl.Phys. A **807**, 214 (2008).
- [16] R.Shyam and U.Mosel, Phys.Rev. C**67**, 065202 (2003).
- [17] R.Shyam and U.Mosel, Phys.Rev. C**79**, 035203 (2009).
- [18] L.P.Kaptari and B.Kaempfer, Nucl.Phys. A**764**, 338 (2006).
- [19] A.P.Jerusalimov, G.I.Lykasov, Int.J.Mod.Phys. A **32**, 01031 (2017); arXiv:1704.00311 [hep-ph].
- [20] A.P.Jerusalimov, G.I.Lykasov, Phys.Part.Nucl. Lett. **15**, 457 (2018).
- [21] F.A. Berends, A. Dannache, D.L. Weaver, Nucl.Phys. B **14**, 1 (1967).
- [22] Yu.S. Surovtsev, T.D. Blokhintseva, P. Bydzôvsky, N. Nagy, Phys.Rev. C **71**, 055205 (2005).
- [23] A.P. Jerusalimov et al., Eur.Phys.J. A**51**, 83 (2015).
- [24] B.Ramstein et al., HADES Collaboration, Eur.Phys.J. Web Conferences, **199**, 01008 (2019).
- [25] D.J. Herndon et al. PR D **11**, 3165 (1975).
- [26] D.M.Manley and E.M. Saleski, PR D**45**, 4002 (1992).

- [27] A.F.Krutov, R.G.Polegaev, V.E.Troitsky, Phys.Rev. D93, 036007 (2016).
- [28] A.Antognini, et. al., Science, 339, 417 (2013).
- [29] S.Ph. Bereznev, et.al., Sov.J.Nucl.Phys. **24**, 591 (1976).
- [30] HADES, B.Ramstein, et al., Eur.Phys.J. Web Conf. **199**, 2012 (2019).